Advances in Water Resources 116 (2018) 167–177

Contents lists available at ScienceDirect

Advances in Water Resources

journal homepage: www.elsevier.com/locate/advwatres

Evaluating drywells for stormwater management and enhanced aquifer recharge

Salini Sasidharan[a,b,*], Scott A. Bradford[b], Jiří Šimůnek[a], Bill DeJong[c], Stephen R. Kraemer[d]

[a] Department of Environmental Sciences, University of California Riverside, Riverside, CA 92521, United States
[b] United States Department of Agriculture, Agricultural Research Service, U. S. Salinity Laboratory, Riverside, CA 92507, United States
[c] Torrent Resources, 9950 Alder Ave, Bloomington, CA 92316, United States
[d] Systems Exposure Division, National Exposure Research Laboratory, Office of Research and Development, US Environmental Protection Agency, Los Angeles, CA, United States

ARTICLE INFO

Keywords:
Drywell
HYDRUS (2D/3D)
Falling head
Inverse simulation
Hydraulic properties
In situ

ABSTRACT

Drywells are increasingly used for stormwater management and enhanced aquifer recharge, but only limited research has quantitatively determined the performance of drywells. Numerical and field scale experiments were, therefore, conducted to improve our understanding and ability to characterize the drywell behavior. In particular, HYDRUS (2D/3D) was modified to simulate transient head boundary conditions for the complex geometry of the Maxwell Type IV drywell; i.e., a sediment chamber, an overflow pipe, and the variable geometry and storage of the drywell system with depth. Falling-head infiltration experiments were conducted on drywells located at the National Training Center in Fort Irwin, California (CA) and a commercial complex in Torrance, CA to determine in situ soil hydraulic properties (the saturated hydraulic conductivity, K_s, and the retention curve shape parameter, α) for an equivalent uniform soil profile by inverse parameter optimization. A good agreement between the observed and simulated water heights in wells was obtained for both sites as indicated by the coefficient of determination 0.95-0.99–%, unique parameter fits, and small standard errors. Fort Irwin and Torrance drywells had very distinctive soil hydraulic characteristics. The fitted value of K_s=1.01 × 10^{-3} m min^{-1} at the Torrance drywell was consistent with the sandy soil texture at this site and the default value for sand in the HYDRUS soil catalog. The drywell with this K_s= 1.01 × 10^{-3} m min^{-1} could easily infiltrate predicted surface runoff from a design rain event (~51.3 m^3) within 5760 min (4 d). In contrast, the fitted value of K_s=2.25 × 10^{-6} m min^{-1} at Fort Irwin was very low compared to the Torrance drywell and more than an order of magnitude smaller than the default value reported in the HYDRUS soil catalog for sandy clay loam at this site, likely due to clogging. These experiments and simulations provide useful information to characterize effective soil hydraulic properties in situ, and to improve the design of drywells for enhanced recharge.

1. Introduction

Water has a strong influence on food and energy production, industrial and agriculture output, and population and economic growth of nations (Gleick, 1993; Shannon et al., 2008). The availability of high-quality water resources is rapidly decreasing, especially in arid and semi-arid regions of the world, due to the demographic shift and the subsequent increase in demand and overuse of freshwater, and contamination of aquifers and lakes (Shannon et al., 2008; Koehler, 2008). Climate variability has further increased the vulnerability of water resources and it is estimated that around 5 billion people will be living in countries under water stress by 2025 (Treidel et al., 2011; Vorosmarty et al., 2000; Arnell, 1999). In addition, urban development with paved and impermeable surfaces has had a profound impact on the hydrologic cycle by altering drainage patterns, reducing infiltration and water storage, and increasing the volume of surface runoff (Dunne and Leopold, 1978; Mount, 1995). This can contribute to a decline in natural groundwater recharge, long-term and short-term drought, an increase in water pollution levels, and flooding caused by surface runoff (Weng, 2001; Arnold and Gibbons, 1996).

Many arid and semi-arid urban regions of the world face serious challenges in maintaining water quality and quantity to meet its growing population demand. For example, around 60% of the water supply in Southern California is imported from the Colorado River Basin and Northern California, and the rest is withdrawn from its local aquifers (Freeman, 2008). Even though Los Angeles (LA) County collects stormwater runoff from its urban surfaces and uses it for artificial recharge, more than 680 Mm^3 of its urban runoff (equivalent to half of its imported water) reaches the ocean annually (DWR, 2009). How-

* Corresponding author at: United States Department of Agriculture, Agricultural Research Service, U. S. Salinity Laboratory, Riverside, CA 92507, United States.
E-mail address: salinis@ucr.edu (S. Sasidharan).

https://doi.org/10.1016/j.advwatres.2018.04.003
Received 27 November 2017; Received in revised form 26 March 2018; Accepted 7 April 2018
Available online 14 April 2018

ever, local groundwater basins in LA County have more than 1480 Mm^3 of unused storage capacity that could be used to store this untapped freshwater resource. Furthermore, capturing and recharging stormwater into the aquifers will reduce LA County's dependence on imported water, energy needs for pumping, and improve its management of flooding and contaminant loads from surface runoff (Dallman and Spongberg, 2012; MWD 2007; Davis and McCuen, 2005). Consequently, implementation of management practices to capture stormwater and enhance its recharge into aquifers can have a large influence on many water quality and quantity aspects (LACDPW, 2014).

Engineering systems which manage surface water and infiltrate it into aquifers are classified as surface, vadose zone, and direct injection infiltration systems (Bouwer, 2002; Edwards et al., 2016). Surface infiltration systems (e.g., infiltration basins, detention basins, vegetated swales, and managed aquifer recharge ponds) place stormwater directly on the ground surface. They require highly permeable sediment and a large surface area for rapid infiltration to occur but can lose water due to evapotranspiration (Bouwer, 2002). Most of the surface area of vadose zone infiltration systems (e.g., recharge trenches and drywells) extends either vertically or horizontally under the ground surface (Bouwer, 2002; Dillon and Pavelic, 1996). Injection wells (e.g., managed aquifer recharge) are used to transmit water directly into aquifers (Bouwer, 2002; Dillon, 2005). Both injection and vadose zone infiltration systems have no or only minimal evapotranspiration losses, do not require large installation area, and may employ large water ponding depths to facilitate rapid infiltration. These various engineering systems also offer different potentials for reactive contamination transport and attenuation in the vadose zone. Direct injection wells provide no chance for contaminant attenuation in the vadose zone (Bouwer, 2002), whereas vadose zone and especially surface infiltration systems provide opportunities of contaminant removal in the vadose zone (Bouwer, 2002; Edwards et al., 2016; Dillon and Pavelic, 1996). Only vadose zone infiltration systems offer potential advantages of minimal evapotranspiration, small installation area, large ponding depths, and vadose zone treatment.

One vadose zone infiltration system that has gained a lot of recent attention in the United States and around the world is a drywell. Drywells are subsurface storage facilities that receive, temporarily store, and infiltrate stormwater into the vadose zone (Edwards et al., 2016). Modern drywell designs include a fully permeable well that is located above the water table and may have pretreatment systems such as single/double sedimentation chambers to remove sediments and sponges to adsorb hydrocarbons in stormwater (Edwards et al., 2016). In addition to the advantages noted above, drywells are also popular because they have a relatively low installation and maintenance cost in comparison to other engineered infiltration systems. However, drywells are not well suited for areas with low permeability soils, high water tables, steep slopes, or contaminated soils (landfills and industrial complexes) due to the potential risks of groundwater pollution (LACDPW, 2014). Furthermore, drywell failure may occur due to clogging if pretreatments are inadequate or in situ clays are mobilized. In this case, a complete reconstruction or a new drywell may be required.

Limited published research has examined the performance of drywells (Edwards et al., 2016; Jurgens et al., 2008; Izuka, 2011). Snyder et al. (1994) reported on a drywell recharge study in the Portland Basin in Oregon, USA, and found that 5700 drywells in urban areas contributed 38% of the total recharge to groundwater within the basin. Wilson et al. (1990) analyzed the impact of drywells on recharge, groundwater pollution, and urban runoff at three sites in Arizona. Results indicated that recharge from drywells created a transmission zone for water movement with minimal impacts on groundwater quality. In contrast, field and numerical modeling studies in Washington and Arizona, USA demonstrated that pollutant attenuation was related to the soil particle size, and recommended that drywells be located in soil profiles with a clay layer to enhance contaminant adsorption (Adolfson-Associates, 1995; Bandeen, 1984). The above considerations suggest that, even if previous results are encouraging, more research is needed to better understand the impact of drywells on groundwater recharge and quality.

Knowledge of the soil profile hydraulic properties is essential for the successful design, execution, and long-term operation of a potential drywell location. Bandeen (1987) simulated the variably-saturated subsurface flow from a drywell using an axísymmetric flow domain and the Galerkin finite element method that was implemented in the Unsat2 program. Water flow from the drywell was represented as a gravel filled borehole. The soil hydraulic properties were determined from a constant borehole infiltration test and empirical formula (Bandeen, 1984; Bandeen, 1987). However, existing numerical models have not yet accurately represented the complex geometry of modern drywell designs, like MaxWell Type IV (Torrent Resources), which includes an upper sedimentation chamber, an overflow pipe, and a bottom chamber packed with gravel that determine the total volume and the maximum head of the drywell. Consequently, these models will not accurately simulate the filling and falling head cycle within a modern drywell, subsequent infiltration into the vadose zone, and determination of the effective soil hydraulic properties via inverse optimization. To our knowledge, there is no existing literature or numerical modeling on determining average soil hydraulic properties using the inverse optimization of field-scale falling head data in a modern drywell system.

The main objective of this study was to improve our understanding and ability to characterize the drywell behavior by conducting systematic numerical and field-scale experiments. The HYDRUS (2D/3D) computer software was modified to simulate transient head boundary conditions for the complex geometry of a modern drywell; i.e., a sediment chamber, an overflow pipe, and the variable geometry and storage of the drywell system with depth. Falling-head experiments were conducted at drywells (MaxWell IV model, Torrents Resources, Arizona, USA) located in the National Training Center in Fort Irwin, California and a commercial complex in Torrance, California. The effective soil hydraulic parameters with the saturated hydraulic conductivity, K_s, and the retention curve shape parameter, α, for an equivalent uniform soil system representative of both sites were determined by inverse parameter optimization of the observed falling head data. Comparison of the fitted K_s and α parameters from these two distinctive sites provide useful information to characterize and improve the design of the drywells.

2. Materials and methods

2.1. Field sites

The drywell in the first study (June 2017) is situated at the Sleepy Hollow Military Housing within the Fort Irwin National Training Center (NTC) in the Mojave Desert, California (CA) (Fig. 1(A)). The Fort Irwin base climate is typical of the Mojave Desert with low precipitation, hot summers, and cool winters (Densmore and Londquist, 1997). It has an annual precipitation of roughly 0–13 mm. Summer monsoon thunderstorms may bring heavy (intensity and depth) rainfall over a small area, which can cause localized flooding (Higdon, 2004; Hubbard, 2013). The NTC receives its water from local aquifers, including the Irwin Basin that is underneath the cantonment area. The Army Net Zero Water program has a long-term goal to balance water pumping with aquifer recharge. A drywell was installed on a portion of the cantonment area of Fort Irwin, adjacent to four softball fields, referred to as the Four-Plex Site (see Fig. 1(A)) in 2007. Urban runoff generated from housing developments upstream of the Four-Plex site is directed into a detention pond where the drywell is located.

The drywell in the second study (September 2017) is situated in a commercial complex in Torrance, the Los Angeles County, California (Fig. 1(B)). The tested drywell was part of a four drywell system installed in May 2013 at this site as a Standard Urban Stormwater Mitigation Plan requirement (SUSMP). The SUSMP was developed as part of the municipal stormwater program to address stormwater pollution

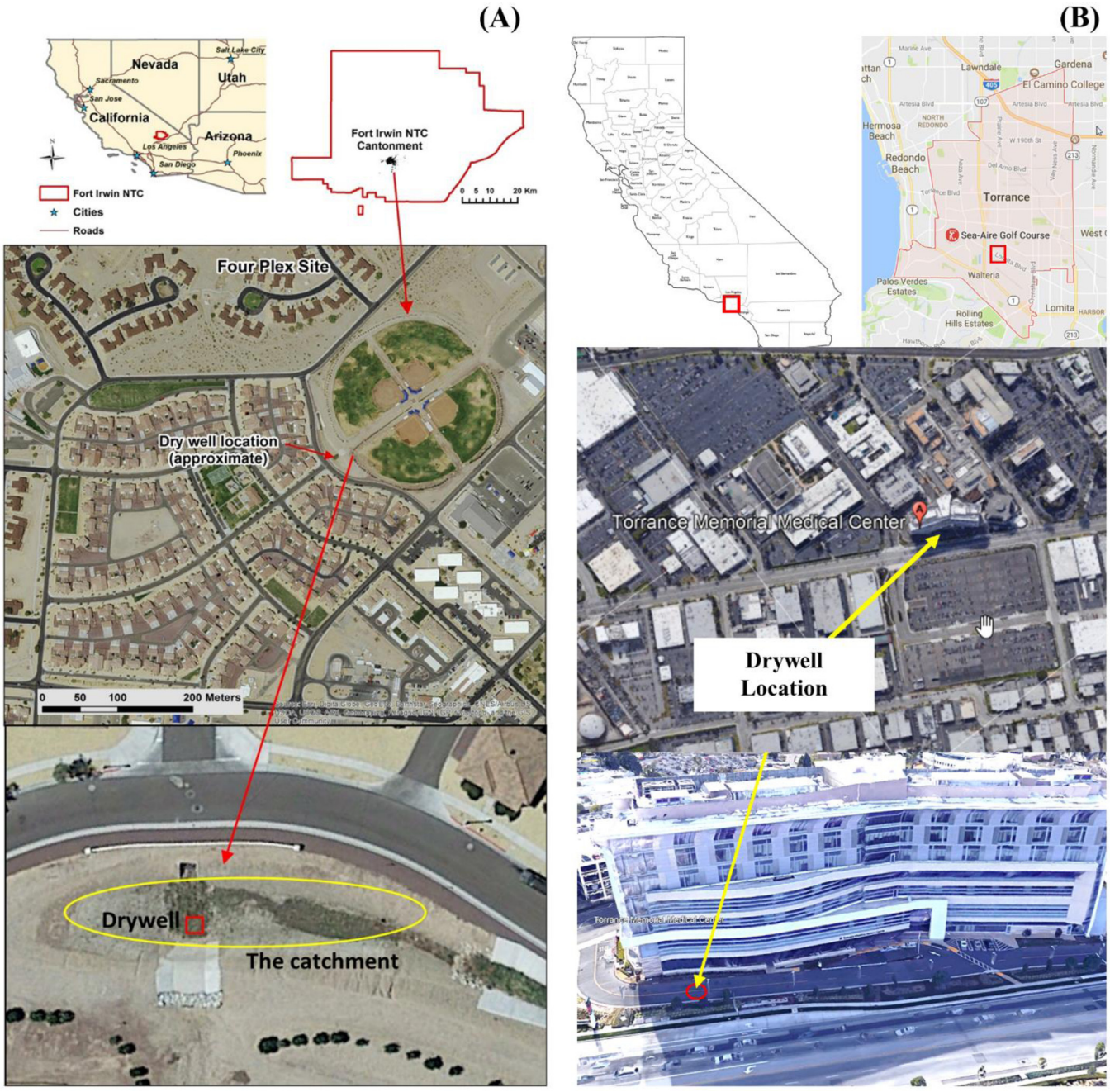

Fig. 1. (A) The Fort Irwin National Training Center located in California, a portion of the cantonment area within Fort Irwin referred to as the Four-Plex Site, and the approximate location of the drywell. (B) A commercial complex situated in Torrance, the Los Angeles County in California, and the location of the drywell.

from development projects (LA-Stromwater, 2000). The site drainage area is about 3.21 acres, with ~90% impervious surface, and the drywell receives pre-treated (StormFilter, Contech Engineered Solutions) water from subsurface piping (DeJong, 2017).

2.2. Drywell engineering design

The MaxWell IV model (Torrents Resources, Phoenix, Arizona, USA) drywell was installed at Fort Irwin and Torrance. Figs. S1A and S1B show the engineering designs for the Fort Irwin and Torrance drywells, respectively. The Fort Irwin and Torrance drywells receive inflow water into an upper sediment chamber through a grated opening on top and subsurface detention pipes, respectively. This upper sediment chamber has an impermeable chamber side, a concrete base seal, and a floating hydrocarbon capture pillow, which removes a wide range of hydrocarbons. Silt, sediment, and debris settle out of the water by gravity inside the upper chamber. Incoming water rises inside the upper sediment chamber and then enters an overflow intake pipe which is connected to a lower chamber. The overflow inlet is equipped with a debris screen, which blocks the passage of suspended matter and other floating debris. Water from the overflow pipe enters a lower chamber, which is filled with clean rocks (0.9–3.8 cm). The entire gravel pack is surrounded by a fully permeable (needle punched) non-woven geotextile (polypropylene or polyester) fabric sleeve to prevent the migration of fines into the gravel pack. Water in the gravel pack infiltrates into the vadose zone soil envelope and eventually recharges groundwater aquifers (TorrentResources, 2012).

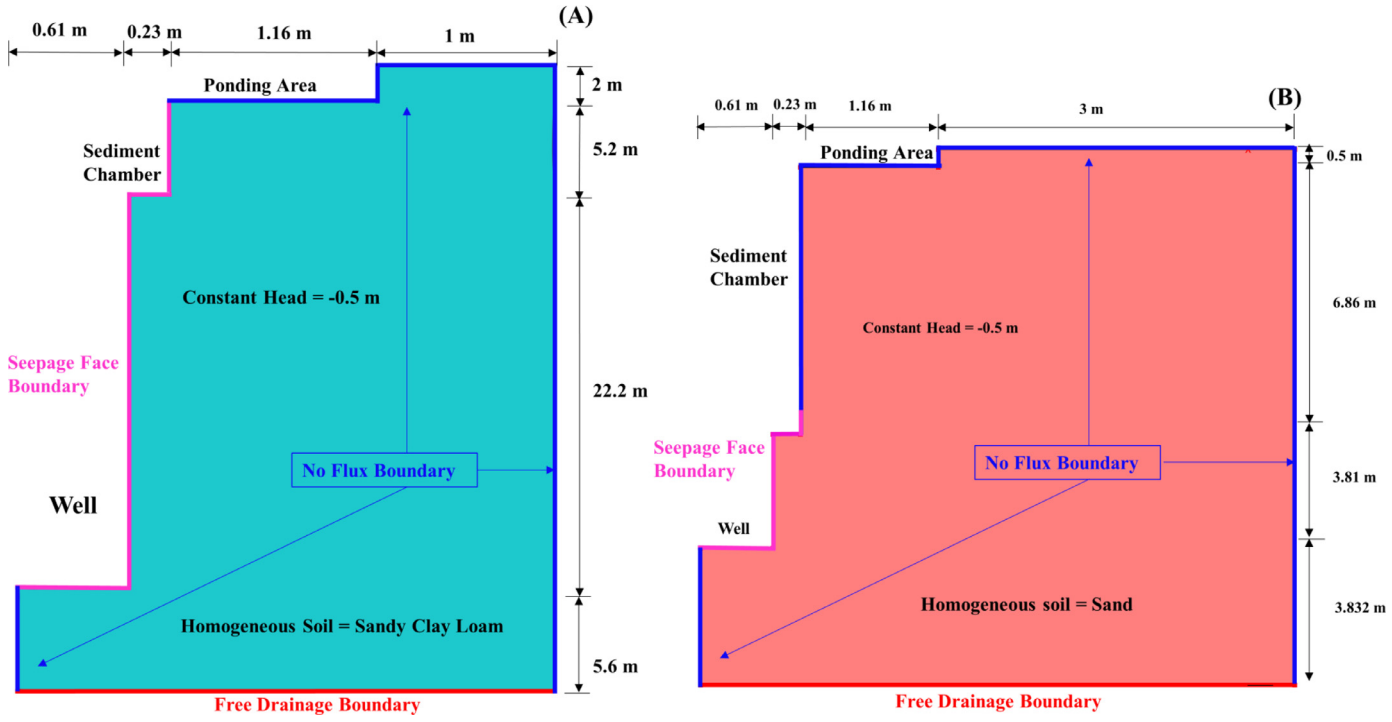

Fig. 2. The geometry of the flow domain, boundary conditions, and initial conditions used during simulations of a homogeneous system representing (A) the Fort Irwin Drywell and (B) the Torrance Drywell.

2.3. Falling head infiltration experiment

A fire hydrant was used to flood the detention pond to fill the Fort Irwin drywell. A vacuum pump truck was used to remove excess water from the detention pond until the water level just reached the top of the grate covering the entrance to the drywell. The detention pond was partially filled for 163 min. At this point, a calibrated pressure transducer (Decagon CTD-10 sensor 40683, USA) was lowered into the bottom of the upper sediment chamber and used to measure the water depth in the drywell every minute with an accuracy of 0.05% and resolution of 2 mm. This pressure transducer was connected to a data logger (Decagon Em50 Series) and then to a laptop computer via a USB cable. When the water level reached the inlet of the overflow pipe (at 60 min), the pressure transducer was moved into the overflow pipe and lowered to a depth of 10 m from the surface and the water level was monitored for 1098 min. According to the engineering design, the sediment chamber wall (the bottom section of the concrete liner with a small number of side perforations) and the base (solid concrete slurry) are impermeable and should thus allow infiltration at a much smaller rate than the bottom of the well. However, we observed that the entire drywell system, i.e., the sedimentation chamber and the well bottom, acted like a single system and drained at the same rate. This indicates that the base concrete slurry seal might have broken and allowed water to flow directly into the bottom chamber. The final water level measurement was taken at 1481 min using a Model 102 Water Level Meter (Solinst Canada Ltd., Canada) with a resolution of 1 mm (Solinst, 2017). A small amount of water was released into the drywell during the night hours from sprinkler irrigation runoff, and the resultant change in pressure head was recorded by the pressure transducer (Table S4).

A calibrated pressure transducer (Decagon CTD-10 sensor 40683, USA) was placed at the bottom of the Torrance, CA, drywell via the overflow pipe. The experiment was conducted in three phases. In Phase I (0–74 min), a fire hydrant outlet that was connected directly to the upper sediment chamber was used to fill this shallow drywell system (0–7 min) (only 10.67 m depth) in a controlled manner. Falling head measurements (7–74 min) were recorded using the pressure transducer (every minute) and a datalogger (Decagon Em50 Series) until the water level in the well reached a steady state. In Phase II (75–98 min), a constant head test was conducted by refilling the drywell and then maintaining the head by adjusting the inflow using a flowmeter connected to the fire hydrant outlet. In Phase III (99–154 min), the drywell was completely refilled and a second falling head test was conducted (Table S4). During our site visits, we have measured the dimensions of the Fort Irwin and Torrance drywells and this information is given in Figs. S1A and S1B.

3. Numerical modeling

The HYDRUS (2D/3D) software package is a finite-element model for simulating the two- or three-dimensional movement of water, heat, and multiple solutes in variably saturated media (Simunek et al., 2016). Water flow is described in HYDRUS (2D/3D) using the Richards equation:

$$\frac{\partial \theta}{\partial t} = \frac{\partial}{\partial x_i}\left[K\left(K_{ij}^{A}\frac{\partial h}{\partial x_j} + K_{iz}^{A}\right)\right] \quad (1)$$

where θ [L^3 L^{-3}, dimensionless, L denotes units of length] is the volumetric water content, h [L] is the pressure head, x_i (i = 1, 2) [L] are spatial coordinates, t [T, T is unit of time] is time, K_{ij}^{A} are components of a dimensionless hydraulic conductivity anisotropy tensor K^A, and K [L T^{-1}] is the unsaturated hydraulic conductivity function given as the product of the relative (K_r) and saturated hydraulic conductivity (K_s) [L T^{-1}].

The unsaturated soil hydraulic conductivity, K (h), and water retention, θ (h), functions are needed to solve Eq. (1). The unsaturated soil hydraulic property models of van Genuchten (1980) and Mualem (1976) were employed for this purpose:

$$\theta(h) = \left\{\theta_r + \frac{\theta_s - \theta_r}{\left[1 + |\alpha h|^n\right]^m}\right\} \quad h < 0 \quad (2)$$

$$\theta(h) = \theta_s \quad h \geq 0 \quad (3)$$

$$K(h) = K_s S_e^l\left[1 - \left(1 - S_e^{1/2}\right)^m\right]^2 \quad (4)$$

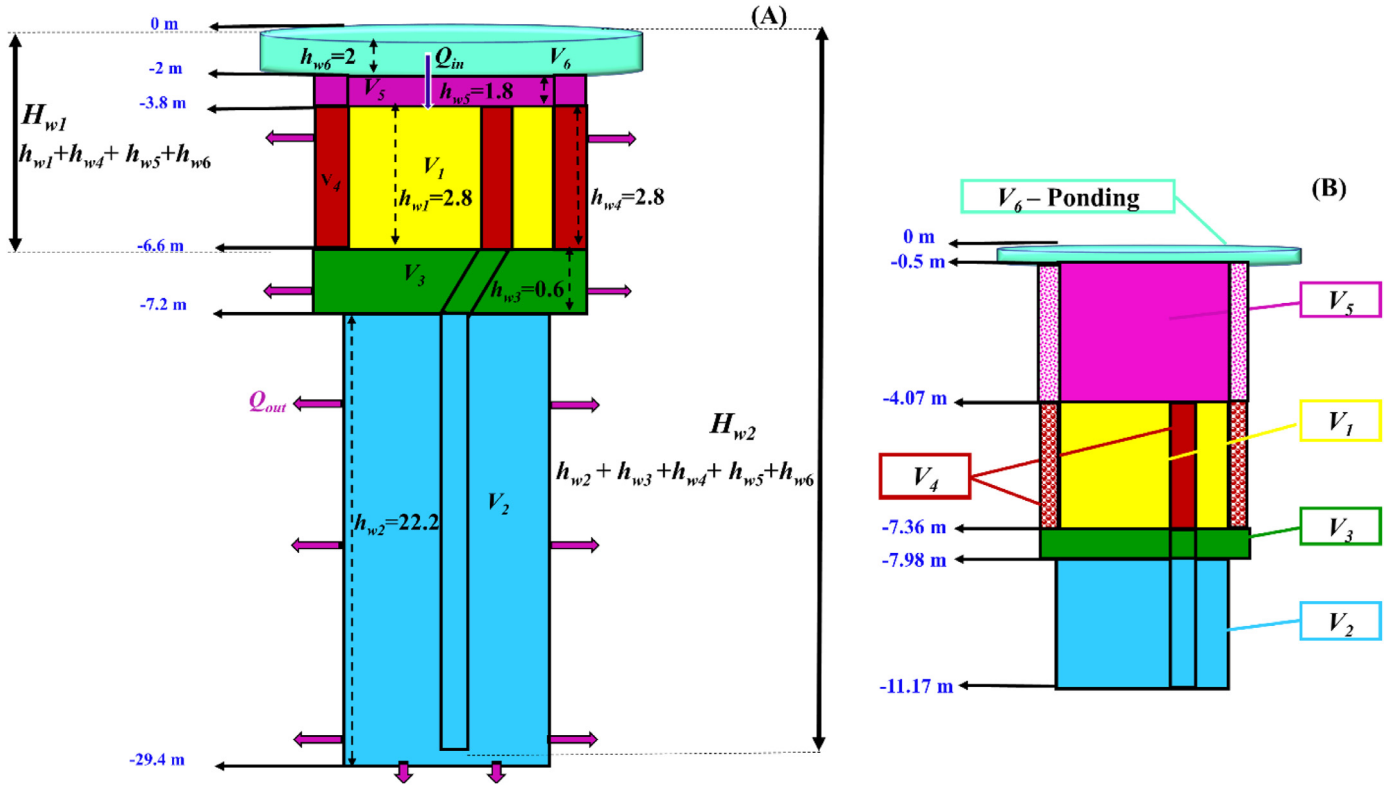

Fig. 3. The geometry of the (A) Fort Irwin and (B) Torrance drywells used in HYDRUS (2D/3D) to simulate infiltration from the drywells. The drywells have 6 reservoirs. Their corresponding maximum water levels and volumes (Vol) are represented as $h_{w1} - h_{w6}$ and $V_1 - V_6$, respectively. Reservoirs 1–5 are parts of the drywell design and Reservoir 6 represents the ponding region above the drywell. Q_{in} is the rate of water inflow into Reservoir 1 and Q_{out} is the rate of water outflow from Reservoirs 2, 3, 4, 5, and 6. The drywell is subdivided into 2 domains: Domain 1 comprised of V_1, V_4, V_5, and V_6 and Domain 2 comprised of V_2, V_3, V_4, V_5, and V_6. H_{w1} and H_{w2} are the water levels in Domain 1 and 2, respectively. Both drywells are implemented as explained above. However, to account for the impermeable region surrounding the sediment chamber in the Torrance drywell (Fig. S1B), a zero porosity was assigned to the shaded region of Reservoir 4 and 5 in Fig. (B).

where θ_r and θ_s [L^3L^3] denotes the residual and saturated water contents, respectively, α [L^{-1}] is the shape parameter in the soil water retention function, l is the pore connectivity parameter, and n and $m = 1–1/n$ are empirical parameters related to the pore size distribution. The effective saturation, S_e, is defined as:

$$S_e = \frac{\theta(h) - \theta_r}{\theta_s - \theta_r} \tag{5}$$

Fig. 2 presents a schematic of the simulation domain, boundary conditions, and initial conditions that were considered for the Fort Irwin and Torrance drywell sites. A 2-dimensional axisymmetrical flow domain was employed in both cases. The Fort Irwin site geometry had a 3-m width and a 35-m depth, whereas the Torrance site had a 5-m width and a 15-m depth. The specified radial dimensions were chosen to best capture the infiltration radius of the drywell based on the soil log information and the vertical dimensions were chosen based on the depth of the drywell. A no-flux boundary condition was assigned to the upper boundary. The nodes representing the right and lower left (the boundary between the drywell and the bottom boundary) sides of the flow domain were set to no flux boundaries. The nodes at the bottom boundary ($z = -35$ m and $z = -15$ m for the Fort Irwin and Torrance drywell simulations, respectively) were assigned a free drainage boundary condition because the groundwater table was deep and below the bottom of the transport domain. Along the left (at $z = -2$ to -29.4 for Fort Irwin and $z = -7.36$ to -11.2 for Torrance) and bottom boundary, a Reservoir Boundary Condition was specified to allow for a seepage face (Šimůnek et al., 2018). For this boundary condition, parts of the boundary that are below and above the water level in the well are internally assigned time-variable pressure head (Dirichlet) and seepage face boundary conditions, respectively. HYDRUS (2D/3D) calculates which part of the seepage face boundary is active (with prescribed zero pressure head) and which is inactive (with prescribed zero flux) depending on whether the boundary nodes are saturated or unsaturated, respectively (Šimůnek et al., 2018). Details pertaining to this so-called Reservoir Boundary Condition are provided in the next section.

The water table at the Fort Irwin and Torrance study site is at approximately 61 and 21 m below the soil surface, respectively. Hence, the distance between the bottom of the drywell and the water table is approximately 34 and 10 m for the Fort Irwin and Torrance drywells, respectively. Therefore, the soil moisture is uniform throughout the domain, the capillary fringe is well below the bottom of the well, and the soil domain surrounding the drywell installation is an unsaturated zone. Hence, the initial condition was specified in terms of the soil water pressure head h (x,z) and was set to a constant pressure head of −0.5 m for the entire domain (Fig. 2).

The simulation domain was discretized into two-dimensional triangular finite element mesh using the MESHGEN tool available within the HYDRUS (2D/3D). The mesh was refined at the left part of the domain where infiltration from the drywell was simulated. To reduce the mass balance error, the finite element grid was adjusted such that the size of elements was smaller (0.05 m) near the well where large water fluxes were expected. The grid size was gradually increased with a radial distance from the drywell, with a maximum element size of 0.75 m and 0.5 m for the Fort Irwin and Torrance domain, respectively. The quality of the finite element mesh was assessed by checking the mass balance error reported by HYDRUS (2D/3D) at the end of the simulation. Mass balance errors were always below 1% and these values are generally considered acceptable (Brunetti et al., 2017).

HYDRUS (2D/3D) includes a parameter estimation procedure based on the Levenberg–Marquardt nonlinear least-squares optimization method (Marquardt, 1963). This procedure was employed to estimate

several unknown parameters in the unsaturated soil-hydraulic functions from measurements of the total water height in the drywells over time by the numerical inversion of the Richards equation. In the absence of detailed information on soil profile heterogeneity (e.g., the soil log does not provide information about the lateral extension of layers), only effective soil hydraulic parameters were obtained for an equivalent uniform soil profile. In particular, the values of α and K_s were determined for the homogeneous soil profile by inverse optimization. Other soil hydraulic parameters (n, l, θ_r, and θ_s) were set equal to default values from the HYDRUS soil catalog for homogeneous Sandy Clay Loam at the Fort Irwin site and Sand at the Torrance site (Table 1). These soil textural classes were chosen based on available soil log information from these sites. Additional research is needed to fully characterize hysteretic hydraulic properties for the heterogeneous soil profiles, but this is beyond the scope of this study.

3.1. Reservoir boundary condition

The drywell has a very complex geometry with multiple compartments. To accurately determine the ponded water height and water flux in the drywell during filling and drainage cycles, the drywell geometry was subdivided into 6 different reservoirs (Fig. 3(A) and (B) for Fort Irwin and Torrance, respectively). Reservoirs 1–5 mimic the drywell design (Figs. S1A and S1B), whereas Reservoir 6 is used to account for external ponding. Geometry parameters for these reservoirs are read into the modified version of HYDRUS from an input file "Well.in". Cross-sectional areas and volumes for each reservoir are subsequently calculated from this information and are provided in Tables S1, S2, and S3. It should be mentioned that the design of drywells at Torrance and Fort Irwin is somewhat different. For example, the sedimentation chamber is much bigger at Torrance (6.9 m) than at Fort Irwin (4.6 m), and Reservoir 2 is much bigger at Fort Irwin (22.2 m) than at Torrance (3.2 m). Furthermore, at Torrance, the gravel pack surrounding the upper sediment chamber was replaced by an impermeable concrete slurry (Fig. S1B) that does not contribute to the volume of Reservoirs 4 and 5 (a zero porosity was assigned to this shaded region in Fig. 3(B)). In contrast to the Fort Irwin drywell's engineering design, we observed that the upper sedimentation chamber had ~1 m thick layer of sediments and the entire drywell system acted like a single system and drained at the same rate. Therefore, additional numerical simulations were conducted by employing the well dimensions obtained from site measurements (Tables S2 and S4).

Fig. 3 indicates that the drywell was subdivided into two main domains. Domain 1 comprises Reservoirs 1, 4, 5, and 6, whereas Domain 2 consists of Reservoirs 2, 3, 4, 5, and 6. The drywell fills from Reservoir 1 to 6. Drainage from Reservoir 1 was not considered since its bottom is covered with an impermeable concrete slurry. Drainage from Domain 2 occurs in the reverse sequence to filling (e.g., Reservoirs 6, 5, 4, 3, and 2). The total water levels (a sum of water levels from reservoirs in Domains 1 and 2; denoted as H_{w1} and H_{w2}) determine which reservoir is actively filling or draining. Logical statements in conjunction with well geometry information were used to determine which reservoir was active at any given time. The initial values of H_{w1} and H_{w2} at the beginning of the simulation $H_{w1}{}^*$ and $H_{w2}{}^*$, respectively, and the water inflow as a function of time, $Q_{in}(t)$ [L^3 T^{-1}], are also input parameters in the "Well.in" file.

The change in the water volume within an active reservoir with respect to time can be calculated using the following mass balance condition:

$$\frac{dV_{wi}}{dt} = A_i \frac{dh_{wi}}{dt} = Q_{in}(t) - Q_{out}(t) \tag{6}$$

where V_{wi} [L^3] is the volume of water in the reservoir, A_i [L^2] is the cross sectional area of the reservoir, h_{wi} [L] is the water level in the reservoir, $Q_{out}(t)$ [L^3 T^{-1}] is the total water outflow to the soil surrounding the drywell, and the subscript i indicates the reservoir number. In its finite

Table 1
Fitted values of the saturated hydraulic conductivity (K_s) and the retention curve shape parameter (α); the standard error (*S.E. Coef*$_\alpha$ and *S.E. Coef*$_{Ks}$), 95% confidence intervals (95% CI_α and 95% CI_{Ks}) for lower (LL) and upper (UL) limits on α and K_s; the coefficient of determination (R^2), and the mass balance error obtained by the inverse simulation for the Fort Irwin and Torrance Drywell.

Site and soil type	Phase /numerical experiment	α [m^{-1}]	*S.E. Coef*$_\alpha$	95% CI_α [LL] [m^{-1}]	95% CI_α [UL] [m^{-1}]	K_s [m min^{-1}]	*S.E. Coef*$_{Ks}$	95% CI_{Ks} [LL] [m min^{-1}]	95% CI_{Ks} [UL] [m min^{-1}]	R^2 [-]	Mass balance error [%]
Fort Irwin (Sandy Clay Loam)	Engineering design	2.63	0.07	2.49	2.77	2.25×10^{-6}	6.29×10^{-9}	2.24×10^{-6}	2.27×10^{-6}	0.96	0.0098
	Onsite measurements	2.42	0.13	2.17	2.68	3.07×10^{-6}	1.06×10^{-7}	2.86×10^{-6}	3.28×10^{-6}	0.95	0.01
Torrance (Sand)	Phase I	0.52	0.04	0.45	0.59	1.17×10^{-3}	4.8×10^{-6}	1.16×10^{-3}	1.18×10^{-3}	0.96	0.31
	Phase II	1.50	0.52	0.41	2.59	1.89×10^{-3}	1.55×10^{-6}	1.32×10^{-3}	5.10×10^{-3}	0.96	0.02
	Phase III	2.80	0.04	2.73	2.87	1.40×10^{-3}	1.64×10^{-5}	1.37×10^{-3}	1.43×10^{-3}	0.99	0.007
	Phase 1 + II + III	0.85	0.001	0.84	0.85	1.01×10^{-3}	2.59×10^{-6}	1.01×10^{-3}	1.02×10^{-3}	0.97	0.05

Note: Default values of the residual soil water content (θ_r), saturated soil water content (θ_s), pore-size distribution parameter in the soil water retention function (n), and the tortuosity parameter in the hydraulic conductivity function (l) in the HYDRUS (2D/3D) Soil Catalog were employed for Sandy Clay Loam and Sand at the Fort Irwin and Torrance sites, respectively. In particular, $\theta_r = 0.1$, $\theta_s = 0.39$, $n = 1.5$, and $l = 0.5$ for Sandy Clay Loam, and $\theta_r = 0.045$, $\theta_s = 0.43$, $n = 2.68$, and $l = 0.5$ for Sand.

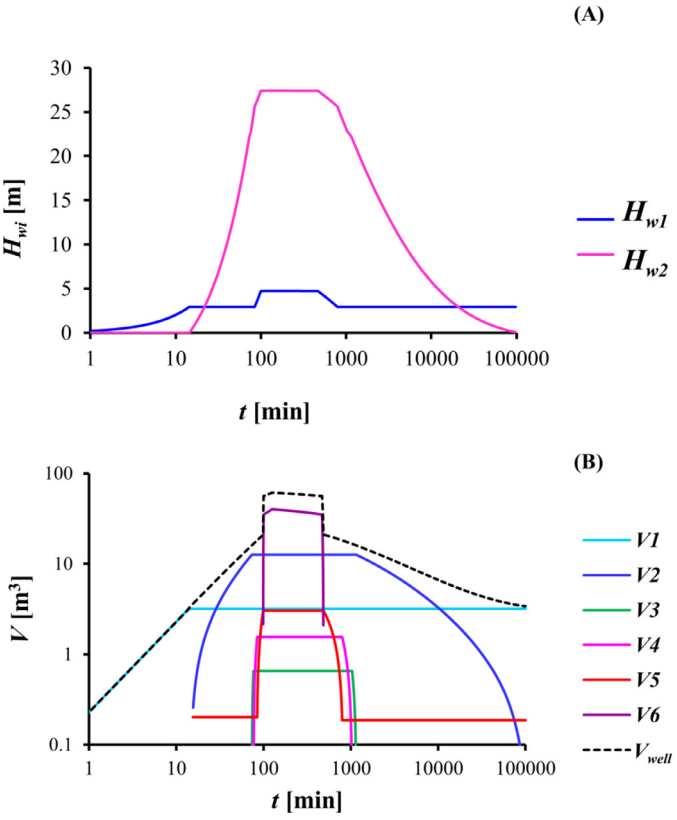

Fig. 4. The Fort Irwin drywell experiment. (A) The water level in Domain 1 (H_{w1}) and Domain 2 (H_{w2}) and (B) the volume of water in each Reservoir (V_1–V_6) and the total volume of water in the whole drywell system (V_{well}= V_1+ V_2+ V_3+ V_4+ V_5+ V_6) during a complete injection (filling) and infiltration (emptying) cycle over 100,000 min simulated with fitted soil hydraulic parameters (Table 1) using the drywell Reservoir Boundary Condition in HYDRUS (2D/3D).

difference discretization Eq. (6) becomes:

$$h_{wi}^{j+1} = h_{wi}^{j} + \frac{\Delta t}{A_i}\left(Q_{in} - Q_{out}\right) \tag{7}$$

where Δt [T] is the time step, and h_{wi}^{j+1} [L] and h_{wi}^{j} [L] are water levels in the reservoir at current and previous time steps, respectively. Eq. (7) is used to determine the water level in an active reservoir at the current time step. The values of H_{w1} and H_{w2} are updated based on this information and the boundary conditions in the HYDRUS domain are dynamically adjusted. Values of Q_{out} (used for the next time step) and the total drywell water volume are subsequently calculated in HYDRUS and printed to new output text files "Well.out" and "WellVolume.out", respectively. The value of $H_{w1}{}^{*}$ and $H_{w2}{}^{*}$ and the time-variable boundary conditions used in the inverse simulation for the Fort Irwin and Torrance drywells are given in Table S4.

In addition, numerical experiments were conducted with hypothetical conditions. The first experiments were conducted to understand the dynamics of the drywell and the functioning of the new Reservoir Boundary Condition. In this case, simulations for a complete filling and drainage cycle were conducted for the Fort Irwin drywell geometry (an engineering design) over 100,000 min (Figs. 4 and S2, Table S5). Other simulations were conducted to compare the cumulative infiltration volume between the Fort Irwin and Torrance drywells over 1100 min for a complete drainage cycle and multiple filling and drainage cycles, respectively (Fig. 8). The time-variable boundary conditions used in these experiments are given in Table S5.

4. Results and discussion

4.1. Dynamics of a drywell

The functioning of the newly developed drywell reservoir boundary condition module and its coupling with the HYDRUS (2D/3D) model during one complete filling and drainage cycle was evaluated using the Fort Irwin drywell geometry. A time-variable boundary condition was employed in the simulation as follows: hypothetical water inflow was 0.23 m^3 min^{-1} for 0 to 100 min and 0 m^3 min^{-1} for 100–10,000 min (Table S5). Fig. 4(A) shows the change in H_{w1} and H_{w2}. Fig. 4(B) shows the sequence of filling and draining of Reservoirs 1–6 and the corresponding change in the total water volume in the drywell system (V_{well}). These figures show that V_{well} increased as the injection continued at a slow pace until Reservoirs 1 through 6 were full. At the beginning of the simulation, the water volume in Reservoir 1 (V_1) (as well as the corresponding value of H_{w1}) increased until it reached the maximum volume of 3.185 m^3. During the next stage, water overflowed through the overflow pipe (Fig. S1) and filled sequentially Reservoirs 2 and 3 (V_2 and V_3) while H_{w1} stayed constant and H_{w2} increased. In the next phase, Reservoirs 4, 5, and 6 (V_4, V_5, and V_6) were filled and the corresponding water levels H_{w1} and H_{w2} increased. Once all 6 reservoirs were full, they started draining in the order of V_6, V_5, V_4, V_3, and V_2 (Fig. 4(B)) and the corresponding water levels H_{w1} and H_{w2} decreased with time (Fig. 4(A)). Note that we do not consider draining of V_1 since the sedimentary chamber is surrounded by an impermeable wall and a base seal concrete slurry. Fig. 4 shows that V_{well}, H_{w1}, and H_{w2} increased and reached the maximum during the filling cycle and then started decreasing to a constant value of V_1 and H_{w1}, whereas H_{w2} went down to zero during the draining cycle. Figures S2A (in a normal scale) and S2B (in a log scale) present the change in the well water volume, cumulative infiltration, and the mass balance for the well water volume during one complete filling (injection) and emptying (infiltration/falling head) cycle for the entire drywell.

4.2. Inverse estimation of soil hydraulic properties

Fig. 5 shows the observed and inversely simulated values of H_{w2} over time at the Torrance site. Fig. 5(A)–(D) consider Phases I (initial filling of the entire drywell and then draining of reservoirs 5, 4, 3, and 2), II (refilling of the drywell and the constant head test), III (refilling of the entire drywell, and then draining of reservoirs 5, 4, 3, and 2), and the entire experiment (Phases I, II, and III), respectively. A sudden decrease in H_{w2} occurs during draining of Reservoir 4 during Phases I and III because it holds a very small volume of water (0.1 m^3) compared to the other reservoirs (Fig. 3(B) and Table S1). Table 1 shows the corresponding fitted values of K_s and α, the standard error coefficient, 95% upper and lower confidence interval limits, the coefficient of determination (R^2), and the mass balance errors for each simulation period.

Fig. 5 and the Table 1 show a very good agreement between the observed and simulated values, with R^2 values of 0.96–0.99% and the mass balance error less than 0.3%. Based on these simulations, the value of α ranged from 0.52–2.80 m^{-1} and the value of K_s ranged from 1.01×10^{-3}–1.89×10^{-3} m min^{-1}. Table 1 shows that all fitted parameters were unique with a very small standard error and a narrow 95% confidence interval. During the simulation for each phase, the initial condition was imported from the last time step of the previous phase, and the observed difference in the fitted K_s and α value can be suggested by the variations in the initial condition (pressure head). This result shows that, conducting multiple filling and drainage cycle experiment will help for the accurate estimation of effective hydraulic properties. In addition, we acknowledge that there is a slight deviation in the slope at Phase I and Phase III during emptying of Reservoir 2. We have tried our best to incorporate the engineering design and onsite measurements to describe the drywell's geometry. However, we believe that this discrepancy in the simulated value of H_{w2} is due to variations in the volume of

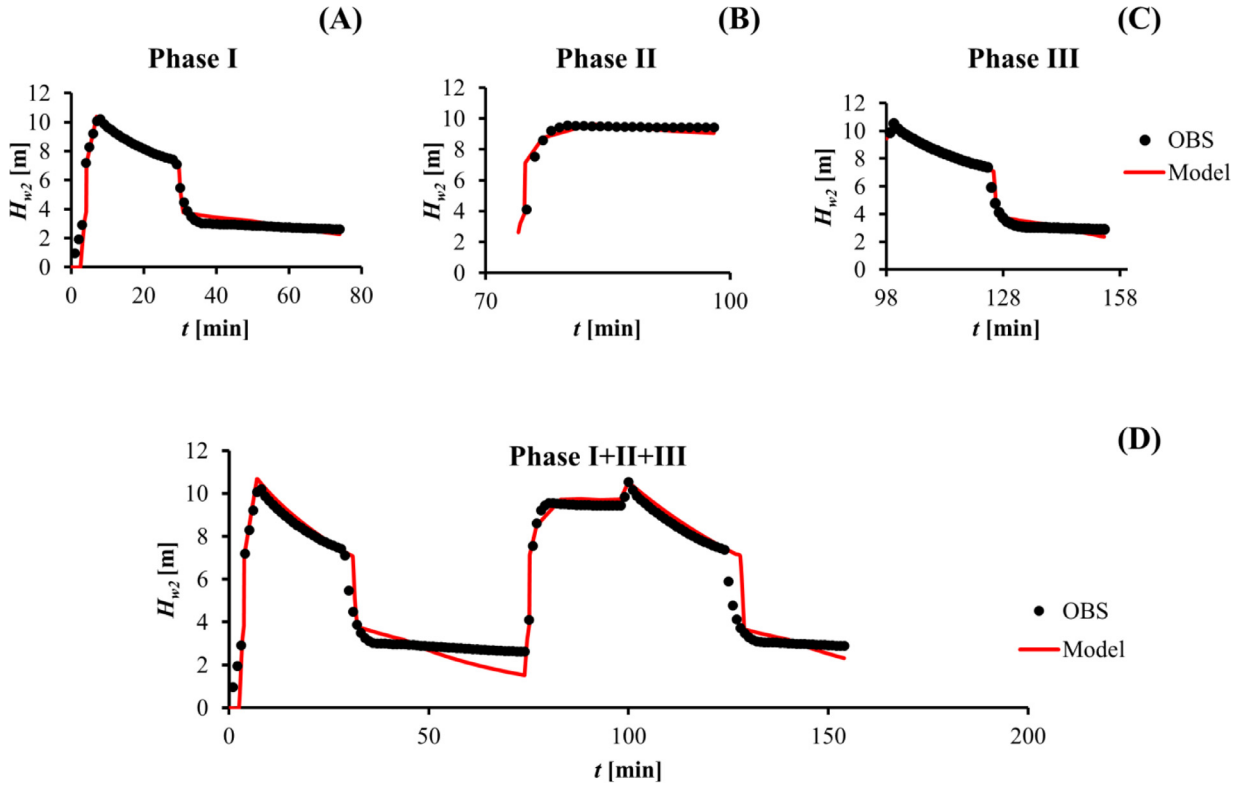

Fig. 5. The Torrance dry well experiment. Observed (black circle markers) and inversely simulated (solid red line) values of pressure heads (H_{w2}) in (A) Phase I (initial filling of the entire drywell, and then draining of Reservoirs 5, 4, 3, and 2), (B) Phase II (refilling of the drywell and the constant head test), and (C) Phase III (refilling of the entire drywell and then draining of Reservoirs 5, 4, 3, and 2). Simulations for each phase were conducted after first importing the initial conditions from the final time step in the previous Phase. (D) The observed and inversely simulated H_{w2} values for the entire infiltration experiment (Phases I, II, and III = 154 min). Table 1 shows the fitted parameters and Table S4 shows the time-variable boundary conditions. (For interpretation of the references to color in this figure legend, the reader is referred to the web version of this article.)

the actual well (e.g., slight variations in the well geometry and/or the porosity of the packing material).

Soil log information collected from 4 drywells at the Torrance site showed the presence of a silty clay layer in a depth of 0–7 m, a silty sand layer in 4.87–9.7 m, a sand layer in 5.4–11.6 m, and a silty sand layer in 10.1–14.93 m. However, the lateral continuity of these layers is not known. Fitted values of high K_s were consistent with previously reported values for sandy soils (van Genuchten MT and Yates, 1991; Carsel and Parrish, 1988; Rawls et al., 1982), and were therefore assumed to be controlled by coarse-textured soils at this site. However, fitted values of α were much smaller than the values reported for sandy soils. Indeed, the fitted value of α=0.85 m^{-1} was much closer to the value reported for silt and clay (van Genuchten MT and Yates, 1991; Carsel and Parrish, 1988; Rawls et al., 1982), and was, therefore, assumed to be controlled by fine-textured silt and clay layers at this site. In comparison to K_s, the fitted value of α exhibited much greater standard error coefficients (Table 1). This uncertainty likely reflects differences in the actual and simulated initial conditions, soil heterogeneity, and/or the influence of hysteresis on hydraulic properties, which were not accounted for this simulation.

Fig. 6(A) compares the measured and simulated (based on the drywell dimensions from the engineering design) values of H_{w2} with respect to time at the Fort Irwin drywell site (Table S4). In comparison to the Torrance drywell results, Fort Irwin falling head data show a very slow decrease in H_{w2} with time during the experiment. Very good agreement between the observed and simulated falling head data was observed, including the change in H_{w2} due to irrigation runoff (821–919 min). The total mass balance error was very small (0.0098%) and a high R^2 value of 0.96% was obtained between observed and simulated values. Table 1 presents the fitted hydraulic parameters. A very small value of K_s= 2.25 × 10^{-6} m min^{-1} was obtained. The fitted value for α was 2.63 m^{-1}. Fig. 6(B) compares the measured and simulated (based on the drywell dimensions from onsite measurement) values of H_{w2} with respect to time at the Fort Irwin drywell site. Very good agreement between the observed and simulated falling head data was observed with a total mass balance error of 0.01% and a high R^2 value of 0.95%. Table 1 presents the fitted parameters. The fitted values of K_s (3.07 × 10^{-6} m min^{-1}) and the value of α (2.42 m^{-1}) were very close to the K_s and α values obtained by the previous (engineering design dimensions) simulation. Based on the soil log information, this site contains ~90% sandy clay, which has a reported K_s value in the range from 2 × 10^{-5} to 8.46 × 10^{-5} m min^{-1} (van Genuchten MT and Yates, 1991; Carsel and Parrish, 1988; Pachepsky and Park, 2015). This observation suggests that other factors (e.g., clogging) may have contributed to the fitted K_s value for this site, which is more than an order of magnitude lower than the default value for sandy clay loam in the HYDRUS soil catalog. Soil log information collected from the Fort Irwin site showed the presence of a sandy clay layer in a depth of 0–5.2 m, a sandy loam layer in 5.2–7.6 m, a sandy clay layer 7.6–20.7 m, a sand layer in 20.7–21.6 m, and a sandy clay layer in 21.6–33 m. However, the lateral extension of these highly permeable sand and sandy loam layers is not known and we assume that it must be very small based on the observed falling head data and the fitted K_s value. The fitted value of α falls in the range of reported values for sandy clay loam (2.7 m^{-1}) (van Genuchten MT and Yates, 1991; Carsel and Parrish, 1988). Therefore, the increased exposure of the Fort Irwin drywell to more sandy clay layers explains the value of α. Our results show that the new Reservoir Boundary Condition implemented in the HYDRUS (2D/3D) model is very flexible and can account for various drywell designs.

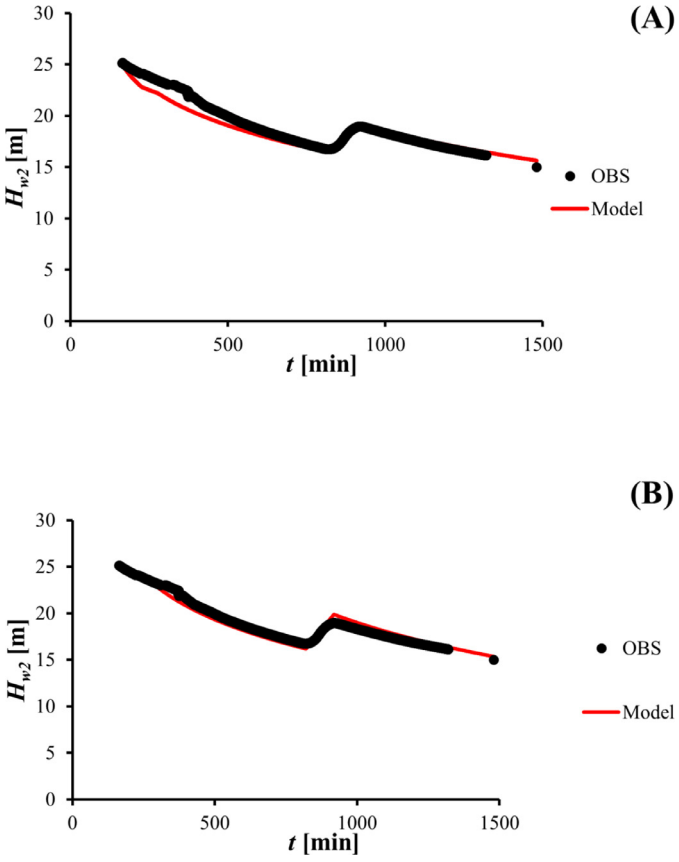

Fig. 6. The Fort Irwin drywell infiltration study. Observed (black circles markers) and inversely simulated (a solid red line) pressure head (H_{w2}) changes over time for the inverse simulation conducted by employing (A) Torrent Resources' engineering design dimensions during the installation time (2007) and (B) drywell dimensions measured during the site visit (2017). Table 1 shows the fitted parameters, Table S2 shows the well dimensions, and Table S4 shows the time-variable boundary conditions. (For interpretation of the references to color in this figure legend, the reader is referred to the web version of this article.)

4.3. *Predicted* h *and θ distributions*

Figs. 7 and S3 show simulated spatial h and θ distributions, respectively, in the model domain for the Torrance and Fort Irwin drywell sites after 154 and 1481 min, respectively. A very significant change in h and θ occurs over a large area in the model domain for the Torrance drywell site after 154 min. In particular, the wetting front reached 3.3 m in the vertical direction and 15 m in the lateral direction (i.e., the maximum vertical and lateral extensions of the domain from the bottom point of the well). In contrast, spatial changes in h and θ occur over a much smaller region at the Fort Irwin drywell site after 1481 min. The wetting front reached a depth of 1 m in the vertical direction and 1.19 m in the lateral direction.

4.4. *Cumulative infiltration behavior at drywell sites*

Additional simulations were conducted to better understand the cumulative infiltration behavior at drywell sites. Fig. 8 shows cumulative infiltration at the Torrance and Fort Irwin drywell sites when using calibrated unsaturated soil hydraulic parameters (Table 1) and time-variable input boundary conditions from Table S5. The total simulation time was 1100 min. Multiple filling and draining cycles using a hypothetical water inflow rate of 1.6 m^3 min^{-1} were considered at the Torrance site (5 of them) (Table S5), whereas only a single cycle (falling head) was employed at the Fort Irwin site due to its much lower value of K_s (Tables 1 and S5).

Fig. 8 indicates that the Torrance drywell manages to infiltrate ~53.2 m^3 of water within 1100 min. The Los Angeles County Low Impact Development standard for drywells indicates that there should be no standing water within 5760 min (4 days) of a design rain event (LACDPW, 2014). A design rain event of 1.9 cm h^{-1} for one hour (an average recurrence interval of 5 years) (Atlas, 2018) on 3.21 acres (with a 90% impervious surface) at the Torrance site will contribute ~205 m^3 of water to 4 drywells present at this site, or ~51.3 m^3/drywell (LACDPW, 2014). Thus, the Torrance drywell site can easily infiltrate the expected incoming volume of water from a design rain event within the required time.

The Fort Irwin drywell can only infiltrate ~12.6 m^3 of water within 1100 min (Fig. 8). This infiltrated water volume is much smaller than that for the Torrance site, even though the infiltration area and a ponding depth for the Fort Irwin drywell are much larger (Fig. S1). A design rain event of 2 cm h^{-1} (an average recurrence interval of 10 years) (Atlas, 2018) on 56.9 acres (with a 44% impervious surface) will contribute ~3643.1 m^3 to the Fort Irwin drywell. A simple calculation using the simulated infiltration volume, i.e., ~12.6 m^3/1100 min from Fig. 8, indicates that it will take ~220 days to infiltrate this design rain event volume (3643.1m^3). Not surprisingly, maintenance contractors at Fort Irwin have reported ponding at the drywell site for several months after a storm event (personal communication). This observation confirms that the drywell site has a very small hydraulic conductivity and the well is likely clogged and damaged.

A number of factors provide convincing evidence that clogging has significantly contributed to the low saturated hydraulic conductivity at the Fort Irwin site. For example, sediment and floating objects such as plastics and leaves entered the sediment chamber via the lid and passed through the open overflow pipe into the bottom well during the infiltration experiment, which mimics a natural storm event. The debris shield that goes on top of the overflow pipe was found on the upper sediment chamber floor at the start of the infiltration experiment (Fig. S4). Finally, a comparison of the drywell dimensions using engineering design and our direct measurements shows that there is at least 1–2 m of sediment at the bottom of the upper sediment chamber (Reservoir 1) and the well (Reservoir 2).

5. Summary and conclusions

Field-scale falling head and infiltration experiments were conducted at the Torrance and Fort Irwin drywell locations. These two drywells encompass very different characteristics. The Torrance drywell was much smaller in depth, the soil was highly permeable, the drywell was situated in an urban setting with mainly impervious surfaces covering the soil, incoming water was pretreated via a stormwater filter and large sediment chamber, and the drywell was routinely maintained and functioning according to design standards. In contrast, the Fort Irwin drywell was much larger, the soil had low permeability and was likely clogged, the drywell was situated in a rural setting, and it received little or no maintenance and was not functioning within design specifications.

The HYDRUS (2D/3D) model was modified to simulate the complex geometry of the drywell, and a new Reservoir Boundary Condition was implemented to account for time-variable pressure heads and seepage faces in the drywell that are coupled with the vadose zone. The modified HYDRUS (2D/3D) code was run in an inverse mode to estimate the soil hydraulic properties for an equivalent uniform soil profile at the Torrance and Fort Irwin drywell sites and to successfully simulate temporal changes in the infiltration behavior of two completely different drywells. Furthermore, model simulations predicted the spatial and temporal behavior of subsurface water flow at these drywell sites.

Additional information regarding different drywell sizes, depths, locations, soil heterogeneity, engineering designs, and various contaminant and sediment loadings during individual storms and for a long-

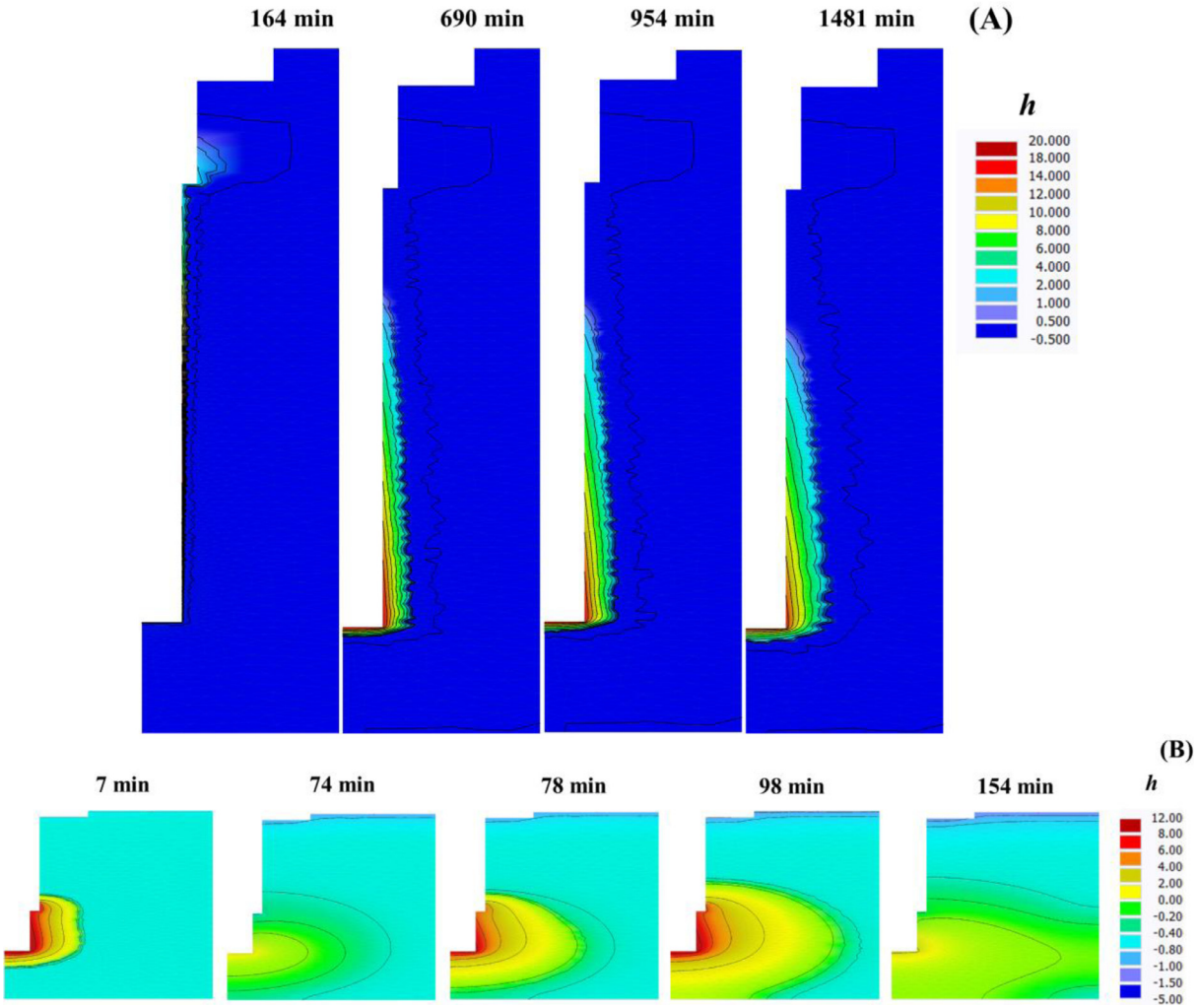

Fig. 7. The soil water pressure head (***h***) profile during the falling head infiltration test at (A) t = 164, 690, 954, and 1481 min at the Fort Irwin drywell and (B) t = 7, 74, 78, 98, and 154 min at the Torrance drywell.

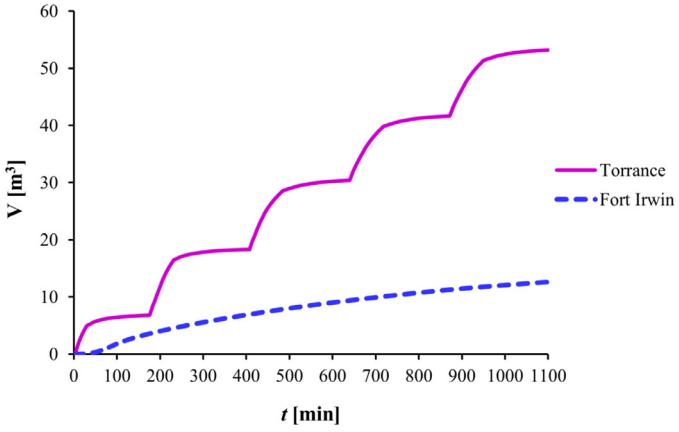

Fig. 8. A comparison of the cumulative infiltration volume for the Torrance and Fort Irwin sites when using fitted hydraulic parameters from Table 1 and the time-variable boundary conditions from Table S5.

term (multiple years) data series are important design considerations to evaluate the effectiveness of drywells in comparison other infiltration systems. Future research activities will, therefore, focus on infiltration from a drywell in heterogeneous soil systems, changes in water quality during transport through the vadose zone, the impact of infiltrated water on groundwater quantity and quality, identification of conditions that pose a risk of clogging (a potential reduction in the infiltration capacity) and a reduction in overall drywell performance, and designs that improve the long-term management and sustainability of drywell injection.

Competing financial interest

None.

Acknowledgment

Funding for this research was provided by the U.S. Environmental Protection Agency (US EPA) through an interagency agreement with the United States Department of Agriculture (EPA DW-012-92465401; ARS 60-2022-7-002). The views expressed in this article are those of the authors and do not necessarily represent the views or policies of the U.S. Environmental Protection Agency. Mention of commercial products does not constitute an endorsement. The data supporting the conclusions can be obtained in the Tables and the Figures available in the supporting information.

Supplementary materials

Supplementary material associated with this article can be found, in the online version, at doi:10.1016/j.advwatres.2018.04.003.

References

Adolfson-Associates, 1995. Pilot Evaluation Subsurface Stormwater Disposal Facilities. Tacoma-Pierce County Health Department, Tacoma-Pierce County Washington.

Arnell, N.W., 1999. Climate change and global water resources. Global Environ. Chang. 9, S31–S49. https://doi.org/10.1016/S0959-3780(99)00017-5.

Arnold, C.L., Gibbons, C.J., 1996. Impervious surface coverage – the emergence of a key environmental indicator. J. Am. Plann. Assoc. 62, 243–258. https://doi.org/10.1080/01944369608975688.

Atlas, N., 2018. Precipitation-frequency Atlas of the United States Accessed on 03/15/ URL:http://www.nws.noaa.gov/oh/hdsc/currentpf.htm.

Bandeen, R.F., 1984. Case Study Simulations of Dry Well Drainage in the Tucson Basin. Water Resources Research Center College of Engineering University of Arizona Tucson, Arizona 85721.

Bandeen, R.F. Additional case study simulations of dry well drainage in the Tucson Basin. Final Report to Pima County Department of Transportation and Flood Control District, June 1987. The University of Arizona Campus Repository, Water Resources Research Center, 1987.

Bouwer, H., 2002. Artificial recharge of groundwater: hydrogeology and engineering. Hydrogeol. J. 10, 121–142. https://doi.org/10.1007/s10040-001-0182-4.

Brunetti, G., Simunek, J., Turco, M., Piro, P., 2017. On the use of surrogate-based modeling for the numerical analysis of Low Impact Development techniques. J. Hydrol. 548, 263–277. https://doi.org/10.1016/j.jhydrol.2017.03.013.

Carsel, R.F., Parrish, R.S., 1988. Developing joint probability distributions of soil water retention characteristics. Water Resour. Res. 24, 755–769.

Dallman, S., Spongberg, M., 2012. Expanding local water supplies: assessing the impacts of stormwater infiltration on groundwater quality. Prof. Geogr. 64, 232–249. https://doi.org/10.1080/00330124.2011.600226.

Davis, A.P., McCuen, R.H., 2005. Stormwater Management for Smart Growth. Springer Science & Business Media.

DeJong, B., 2017. In: Sasidharan, S. (Ed.), Torrance Drywell Engineering Plan. Torrent Resources.

Densmore, J.N., Londquist, C.J., 1997. Ground-water Hydrology and Water Quality of Irwin Basin at Fort Irwin National Training Center. US Departmentof the Interior, US Geological Survey, California.

Dillon, P.J., Pavelic, P., 1996. Guidelines on the Quality of Stormwater and Treated Wastewater for Injection into Aquifers for Storage and Reuse. Urban Water Research Association of Australia.

Dillon, P., 2005. Future management of aquifer recharge. Hydrogeol. J. 13, 313–316. https://doi.org/10.1007/s10040-004-0413-6.

Dunne, T., Leopold, L.B., 1978. Water in Environmental Planning. Macmillan.

DWR, 2009. California Water Plan Update 2009. Department of Water Resources Bulletin. Department of Water Resources, California.

Edwards, E.C., Harter, T., Fogg, G.E., Washburn, B., Hamad, H., 2016. Assessing the effectiveness of drywells as tools for stormwater management and aquifer recharge and their groundwater contamination potential. J. Hydrol. 539, 539–553. https://doi.org/10.1016/j.jhydrol.2016.05.059.

Freeman, G., 2008. Securing Reliable Water Supplies for Southern California. Los Angeles County Economic Development Corporation.

Gleick, P.H., 1993. Water in Crisis: A Guide to the World's Fresh Water Resources. Oxford University Press, Inc..

Higdon, M, 2004. National Training Center (NTC), Fort Irwin, California–A FullYear Climatology, Country Climatological Digest, AFCCC/CCD–04/006. Air Force Combat Climatology Center, National Training Center (NTC), Fort Irwin, California http://irwin-www.army.mil/PdfFiles/USAFWeather/ft.%20irwin%20climo.pdf.

Hubbard, BO, 2013. Corps sends team to Fort Irwin to assess recent storm damage. Engineer Update, U.S. Army Corps of Engineers. Fort Iriwn, Los Angeles District http://www.usace.army.mil/Media/News-Archive/Article/478146/corps-sends-team-to-fort-irwin-to-assess-monsoon-damage/.

Izuka S.K. Potential effects of roadside dry wells on groundwater quality on the island of Hawai'i—assessment using numerical groundwater models. US Geological Survey Scientific Investigations Report. U.S. Geological Survey, 2011. pp. 40.

Jurgens, B.C., Burow, K.R., Dalgish, B.A., Shelton, J.L., 2008. Hydrogeology, Water Chemistry, and Factors Affecting the Transport of Contaminants in the Zone of Contribution of a Public-Supply Well in Modesto, Eastern San Joaquin Valley, California. U. S. Geological Survey.

Koehler, A., 2008. Water Use in LCA: Managing the Planet's Freshwater Resources. Springer.

LA-Stromwater, 2000. Standard Urban Storm Water Mitigation Plan. City of Los Angeles Stormwater Program. LA's Watershead Protection Program, Los Angeles, CA http://www.lastormwater.org/green-la/standard-urban-stormwater-mitigation-plan/.

LACDPW, 2014. Low Impact Development. County of Los Angeles Department of Public Works Standards Manual.

Marquardt, D.W., 1963. An algorithm for least-squares estimation of nonlinear parameters. J. Soc. Indust. Appl. Math. 11, 431–441.

Mount, J.F., 1995. California Rivers and Streams: The Conflict Between Fluvial Process and Land Use. University of California Press.

Mualem, Y., 1976. A new model for predicting the hydraulic conductivity of unsaturated porous media. Water Resour. Res. 12, 513–522.

MWD, 2007. A Status Report on the Use of Groundwater in the Service Area of the Metropolitan Water District of Southern California. Metropolitan Water District of Southern California Groundwater Assessment Study.

Pachepsky, Y., Park, Y., 2015. Saturated hydraulic conductivity of US soils grouped according to textural class and bulk density. Soil Sci. Soc. Am. J. 79, 1094–1100.

Rawls, W.J., Brakensiek, D., Saxtonn, K., 1982. Estimation of soil water properties. Trans. ASAE 25, 1316–1320.

Shannon, M.A., Bohn, P.W., Elimelech, M., Georgiadis, J.G., Marinas, B.J., Mayes, A.M., 2008. Science and technology for water purification in the coming decades. Nature 452, 301–310. https://doi.org/10.1038/nature06599.

Simunek, J, Sejna, M, van Genuchten, MT, 2018. New features of version 3 of the HYDRUS (2D/3D) computer software package. Journal of Hydrology and Hydromechanics 66, 133–142. https://doi.org/10.1515/johh-2017-0050.

Simunek, J., van Genuchten, M.T., Sejna, M., 2016. Recent developments and applications of the HYDRUS computer software packages. Vadose Zone J. 15, 25. https://doi.org/10.2136/vzj2016.04.0033.

Snyder, Daniel T., Morgan, David S., McGrath, Timothy S., 1994. Estimation of ground-water recharge from precipitation, runoff into drywells, and on-site waste-disposal systems in the Portland Basin, Oregon and Washington. Water-Resources Investigations Report, No. 92-4010. US Geological Survey, Earth Science Information Center, Oregon Water Science Center, OR.

Solinst, 2017. Model 102 Data Sheet. Coaxial Cable Water Level Meter. Solinst Canada Ltd., Canada.

TorrentResources. The MaxWell®IV Drainage System Product Information and Design Features. U.S. Patent No. 4923330, 2012, Torrent Resources (CA) Incorporated, Phoenix, Arizona. http://www.torrentresources.com/wp-content/uploads/2014/06/MaxWell-IV-Insert-8-2012_200.pdf

Treidel, H., Martin-Bordes, J.L., Gurdak, J.J., 2011. Climate Change Effects on Groundwater Resources: A Global Synthesis of Findings and Recommendations. CRC Press.

van Genuchten, M.T., 1980. A closed-form equation for predicting the hydraulic conductivity of unsaturated soils. Soil Sci. Soc. Am. J. 44, 892–898.

van Genuchten, M.T., Leij, F., Yates, S., 1991. The RETC code for quantifying the hydraulic functions of unsaturated soils, IAG-DW12933934. U.S. Salinity Laboratory, U.S. Department of Agriculture, Agricultural Research Service, Riverside, California http://citeseerx.ist.psu.edu/viewdoc/download?doi=10.1.1.466.6966&rep=rep1&type=pdf.

Vorosmarty, C.J., Green, P., Salisbury, J., Lammers, R.B., 2000. Global water resources: vulnerability from climate change and population growth. Science 289, 284–288.

Weng, Q., 2001. Modeling urban growth effects on surface runoff with the integration of remote sensing and GIS. Environ. Manag. 28, 737–748.

Wilson, L.G., Osborn, M.D., Olson, K.L., Maida, S.M., Katz, L.T., 1990. The ground-water recharge and pollution potential of dry wells in Pima county, Arizona. Ground Water Monit. Remed. 10, 114–121. https://doi.org/10.1111/j.1745-6592.1990.tb00010.x.